Testing the Correlations Between Low Frequency Quasi-Periodic Oscillations and Spectral Parameters in Black Hole Binaries with *Insight*-HXMT Data

Zhibo Yu (喻知博)[1], Javier García[2], Guglielmo Mastroserio[2], Riley Connors[2], Long Ji (纪龙)[3], Honghui Liu (刘鸿辉)[1], and Cosimo Bambi[1]

Advisor: Cosimo Bambi[1]

1.Center for Field Theory and Particle Physics and Department of Physics, Fudan University, Shanghai 200438, China;

2.Cahill Center for Astronomy and Astrophysics, California Institute of Technology, Pasadena, CA 91125, USA;

3.School of Physics and Astronomy, Sun Yat-sen University, 2 Daxue Road, Zhuhai, Guangdong 519082, China)

Abstract: Low-frequency Quasi-Periodic Oscillations (LFQPOs) are commonly observed in black hole binaries while their physical origin is still unclear. However, observations have revealed that LFQPOs are strongly correlated with spectral properties. In this work, we perform detailed broad-band spectral-timing analysis of the black hole binary MAXI J1820+070 observed by the Hard X-ray Modulation Telescope (*Insight*-HXMT) through its entire 2018 outburst. LFQPOs are detected up to 200 keV during the initial Bright-Hard State (BHS); the QPO frequencies are below 0.5 Hz. The energy spectra in the 2-150 keV band are analyzed through the combination of self-consistent disk-continuum modeling and X-ray reflection spectroscopy. The source presents a stable inner disk radius and the spectral change during the hard state should be attributed to the corona. We show that the sources can be classified into different phases in the BHS as traced on the Hardness-Intensity Diagram. We find a strong correlation between the QPO frequency and powerlaw photon index, and the trend differs among phases. After excluding observations where the corona and disk emission could be directly connected, we identify the corona as the source of LFQPO. We stress that the corona could provide a unified picture of the spectral-timing properties in the system.

Key words: accretion; accretion discs; black hole physics; X-rays: binaries; Astrophysics

1 Introduction

Black hole (BH) low mass X-ray binaries (LMXBs) are binary systems where a stellar-mass BH accretes from a companion star. A considerable portion of gravitational potential energy of the matter is converted into electromagnetic radiation, mostly in the X-ray band. The spectra show a multi-temperature blackbody component generated in the accretion disk, and a power-law component produced by inverse Compton scattering of thermal photons from the disk off free electrons in the so-called "corona", which is some hot, usually compact, medium near the black hole. The disk can also be illuminated by the incident photons from the corona, which results in a reflection component in the observed spectra.

Most BHBs are transient sources with fast and significant variability during their outburst lasting from days to months. The intrinsic time evolution of a BHB can be usually traced in an X-ray hardness-intensity diagram (HID) [1-2]. Depending on the photon flux (low/high) and hardness (hard/soft), observations in different regions in the HID can be classified into different spectral states. The fundamental tool to study the underlying physics of the fast timing variations in BHBs is the power spectral density (PSD), the counterpart of a short segment of the light curve in frequency domain. Low frequency quasi-periodic oscillations (LFQPOs) are narrow peaks in PSDs with frequencies ranging from 0.1 to 30 Hz and are often observed in X-ray binary systems (XRBs) with black holes and neutron stars. This implies a universal physics in the accretion process. LFQPOs can be classified into type-A, -B and -C depending on the frequency ν , amplitude, quality factors Q and background noise in PSDs. The most common type is type-C QPOs, characterized by a strong, narrow peak and is mostly observed in the low/hard states. Other types of LFQPOs are less commonly observed and the peaks are not as significant as type-C QPOs [2].

Models that account for type-C QPOs mainly refer to geometrical effects and waves in the accretion process. [3] first proposed that QPOs result from Lense-Thirring precession of the material in the innermost disk region. [4] extended the model and considered the precession of the inner flow region. Other models consider a constant geometry and suggest the existence of waves near the black hole, including spiral waves in the disk caused by accretion/ejection instability (AEI)[5] and pressure waves in an oscillating corona [6]. See, e.g. [7]. for a more complete review.

Though there is no consensus about the physics behind LFQPOs, it is clear that they strongly depend on spectral properties. Observations have revealed that LFQPOs correlate with Comptonized component[7-8], which is consistent with the common observed positive relationship between LFQPO frequency ν_{QPO} and power-law index Γ of the Comptonized component. It does not eliminate the possibility however, that the disk is the origin of the QPOs if we consider, for instance, oscillations in the properties of the seed photons. Given that, spectral parameters including disk inner radius R_{in}, innermost disk temperature kT_{in}, accretion rate $\dot{M}$, etc. could also be in strong correlation with QPOs. Quantitative analysis of those correlations could potentially probe the underlying physics or test existing QPO models. [9] reported the most stringent measurement of the black hole mass in Cygnus X-1 with an asymptotic linear dependence between ν_{QPO} and Γ adapted from the model in [10]. Such correlations could be alternative tools to determine black hole properties and even provide an opportunity to test QPO models.

MAXI J1820+070 is a bright Low-Mass X-ray binary (LMXB) first discovered at optical wavelength by All-Sky Automated Survey for Super Novae [ASAS-SN; 11] on March 6th, 2018. The follow-up outburst in X-ray was detected by Moni- tor of All-sky X-ray Image[MAXI; 12] six days later. The lightcurve collected by MAXI/GSC shows two sets of "rapid rise and slow decay" patterns with peak luminosity in the 2-6 keV band of about 4 Crab [13], while only in the second set a hard-to-soft transition appears (see Figure 1). There are a number of spectral-timing studies on this source with a variety of instruments. By analyzing data from Neutron star Interior Composition Explorer [NICER; 14],[15] studied this source in the early stage of 2018 outburst with X-ray reverberation techniques, and they concluded a shrinking corona during the Bright-Hard State;[16] studied the Intermediate State with both reflection spectroscopy and Fourier-resolved timing analysis, and the results suggested a vertically expanding corona and a relativistically launching jet. [17] analyzed data in the initial hard state from Nuclear Spectroscopic Telescope Array [NuSTAR; 18] assuming a vertically extended corona, and found the subtle variability is governed by coronal conditions rather than by the inner disk radius. We note that the Chinese X-ray satellite Hard X-ray Modulation Telescope[dubbed as Insight-HXMT; 19] has fast timing capability to capture the QPO signals and broad-band coverage for comprehensive spectral analysis. In this paper, we present a spectral-timing analysis of MAXI J1820+070 with Insight -HXMT data. The observations and data reduction will be described in Section 2. In Section 3, we will show the details of the timing and spectral analysis method, including the extraction of the PSDs and the spectral models utilized in this work. In Section 4, we will discuss and summarize our results.

2 Observations and Data Reduction

The X-ray satellite Hard X-ray Modulation Telescope (*Insight*-HXMT) was launched in 2017 [19]. It covers broad energy band with its three instruments (LE: 1-12 keV; ME: 8-35 keV; HE: 20-250 keV). With short dead times (LE: 1 ms; ME: 250 μs; HE: <10 μs) [20-22] and no pile-up problems for BHBs, it is an ideal facility to conduct a spectral-timing investigation.

There are 144 archived Insight -HXMT observations on MAXI J1820+070 which cover the entire 2018 outburst from MJD 58191 to MJD 58412 (see Figure 1). The observation IDs (hereafter ObsIDs) span from 001 to 154. We use the HXMT Data Analysis Software HXMTDAS ver 2.04 to generate lightcurves and spectra. The background is estimated by standalone scripts hebkgmap, mebkgmap and lebkgmap [23-25]. We screen good time intervals by considering the recommended criteria, i.e., the elevation angle >10 deg, the geomagnetic cutoff rigidity > 8 GeV, the pointing offset angle <0.1 deg, and at least 300 s away from the South Atlantic Anomaly (SAA). The lightcurves are extracted in LE (1-10 keV), ME (10-30 keV), and HE (30-100 keV and 100-200 keV) for timing analysis. For spectral analysis, we fit the spectra of LE in 2-10 keV, ME in 10-30 keV, and HE in 28-150 keV. The 20-24 keV band for ME is also ignored due to the dominating fluorescence lines of silver K-shell detected by the Si-PIN detectors of ME. We group the data with minimum bin size of 100 counts using grppha tool, and add 0.5% systematic uncertainties to all channels.

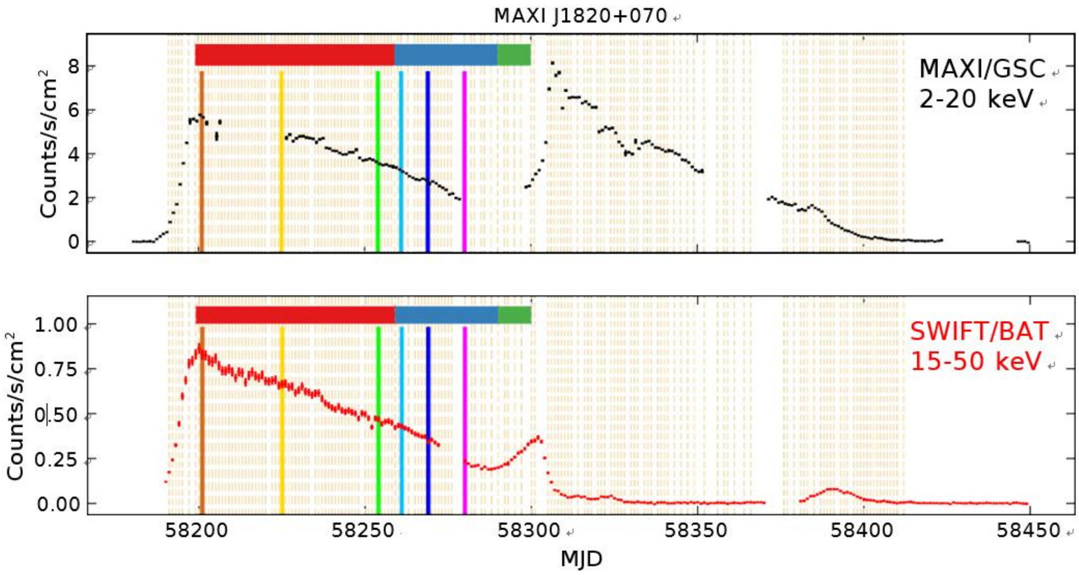

Figure 1. Lightcurves of the 2018 outburst of MAXI J1820+070. Pale-orange vertical dashed lines represent Insight -HXMT observations. Vertical solid lines are observations marked in Figure 4. Red, blue, and green strips on top of the plot represent the “plateau”, “decay”, and “transition” phase, respectively. Top panel: MAXI/GSC 2-20 keV data. Bottom panel: SWIFT/BAT 15-50 keV data.

3 Results

3.1 Timing Analysis

The time resolution of the lightcurves is 1/100 s, corresponding to a Nyquist frequency of 50 Hz, which is sufficient for the study of LFQPOs below 30 Hz. We select observations that contain at least 25 segments to generate the PSDs with Python package Stingray[26] and assume a segment size of 128 s. This corresponds to a minimal frequency of 1/128 Hz. The PSDs are normalized in fractional rms and are rebinned logarithmically with a new frequency bin size increased by a factor of 0.02 compared with the previous bin.

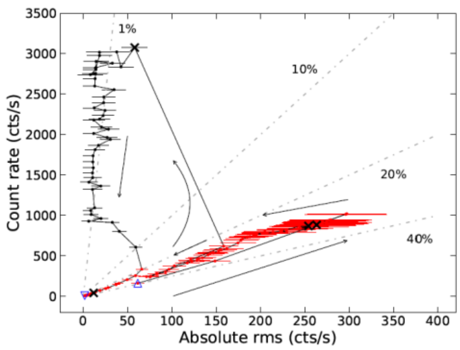

Figure 2. RMS-Intensity diagram of MAXI J1820+070 with Insight -HXMT data. Red points are in hard states. The first and last observations are marked by up triangle and down triangle, respectively. The dashed lines represent different fractional rms values. The arrows show the evolution path of the source. The black crosses mark the observations shown in Figure 3.

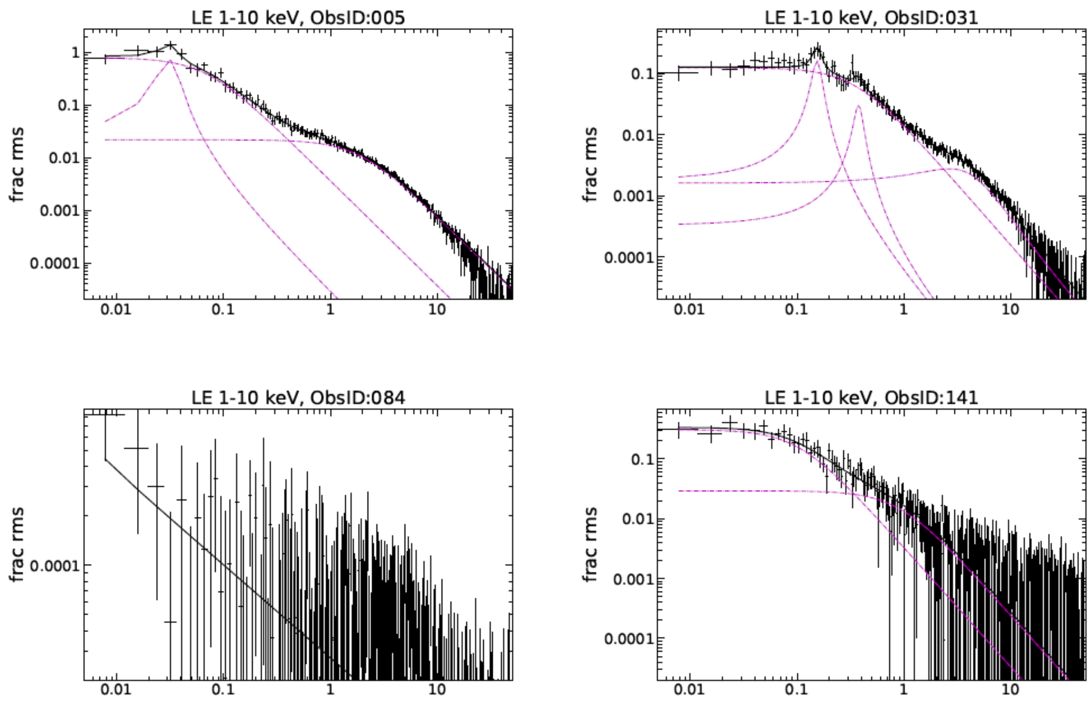

Figure 3. Example of PSDs of LE observations: ObsID 005 and 031 are in the BHS before the transition; ObsID 084 is in the HSS; ObsID 141 is in the LHS towards the end of the outburst.

We classify the states by studying the timing variability. Figure 2 shows the RMS-Intensity diagram. The source begins in Low-Hard State (LHS) and quickly move to Bright-Hard State (BHS). Then its luminosity gradually decreases while the fractional rms remains 30%. After the fast transition into High-Soft State (HSS), the source shows a low variability (1%) and finally moves back to LHS. All PSDs in the hard states are characterized by a flat- topped noise and a high-frequency band-limited noise, and some shows a type- C QPO or even with a harmonic at twice the frequency of the fundamental QPO. We fit these observations with two zero-centered Lorentzians for broad- band noise and one or two narrow Lorentzians to capture the QPO features. For the observations in soft states, the PSDs show a power-law distribution and we fit them with a power-law model. Figure 3.1 shows four characteristic PSDs during the outburst, and the corresponding observations are marked in Figure 2. In all observations we select QPO signals with Q-factor > 3 and detection level > 3σ. There are 61 observations in which significant QPO signals are detected and they are marked in the HID in Figure 3.1. The QPO only appears in the hard state, i.e. the colored region on the upper right corner of the HID. The right panel of Figure 3.1 is the zoomed-in

HID of that region. We further classify different observations in different phases according to the evolution of the source on the HID. After the source reaches its maximum luminosity in the hard state, it gradually softens, which marks the "plateau" phase. Then it enters the "decay" phase when it hardens and the luminosity continues decreasing. After that the source goes into the "transition" phase where it rapidly moves into the HSS.

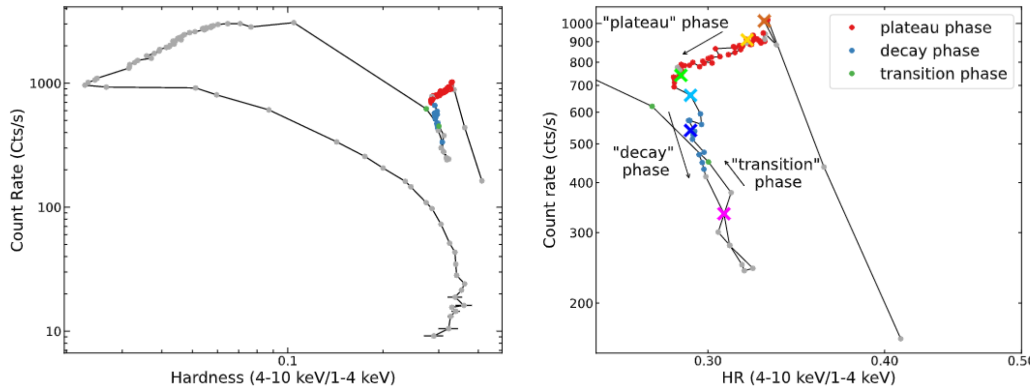

Figure 4. Hardness-intensity diagrams (HIDs) of MAXI J1820+070 with *Insight*-HXMT LE data. Left panel: HID during the entire outburst. Observations in which a QPO is detected are marked by colored points. Right panel: Zoomed-in HID for the observations with QPO. Observations in "plateau", "decay", and "transition" phases are marked by red, blue, and green, respectively. The arrows show the evolution path of the source. The colored crosses represent observations shown in the right panel of Figure 6.

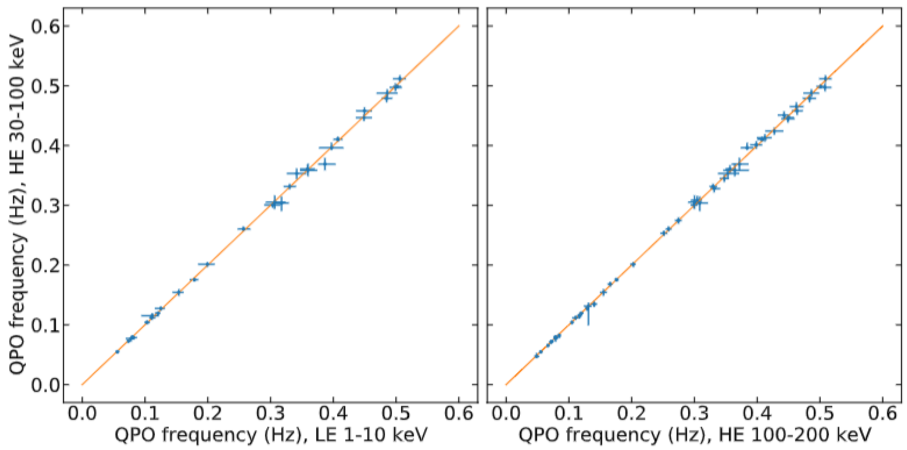

Figure 5. Left panel: ν_{QPO} in LE 1-10 keV band and HE 30-100 keV band. Right panel: ν_{QPO} in HE 30-100 keV and 100-200 keV bands.

We compare the QPO frequencies detected in each energy bands in Figure 5. All QPOs have frequency < 0.5 Hz. There is not any significant discrepancy in the QPO frequency among different energy bands even when we compare the LE results with the HE results. This could be a unique feature of MAXI J1820+070 as in a number of sources the clear energy-dependence of QPO frequency can be observed [7]. For this source, the detected QPO signals are in energy range up tp

200 keV. Such detection in high energy suggests that the QPO signals directly come from the corona, where the high energy photons are produced. This was also reported in [27] where the authors argue that it implies the LFQPO originates from the precession of a small-scale jet. Beyond the authors' approach in timing analysis, we would then conduct the spectral analysis to directly connect the LFQPO with spectral behavior.

3.2 Spectral Analysis

The spectra from the selected 61 observations of MAXI J1820+070 are analyzed. We employ XSPEC v12.11.1 [28] with cross section set to [29] and galactic element abundance set to [30]. We first fit the spectra with an absorbed cut-off power-law: TBabs*cutoffpl. TBabs describes the interstellar absorption and the hydrogen column density nH is the only parameter. We fix $nH = 1.5 \times 10^{21}\ cm^{-2}$ [31]. Figure 6 left panel shows the data-to-model ratio of the best-fit result for ObsID 004 in the BHS. The blurred iron Kα emission line centered at 6.4 keV and the Compton hump at 20-50 keV indicate a relativistic reflection component. A narrow core to the iron emission at 6.4 keV is also seen, which suggest a distant reflection where the region on the disk away from the black hole is illuminated and the reflection is not strongly affected by relativistic effects.

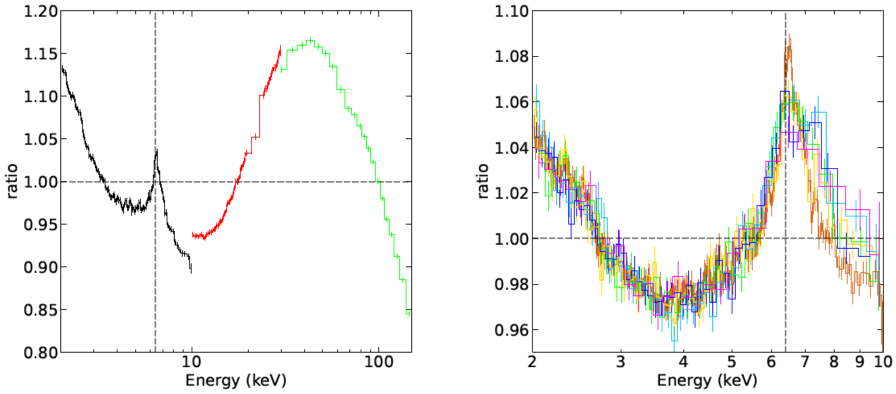

Figure 6. Left panel: Data-to-model ratio plot of ObsID 004 in the BHS. The black, red, and green data points are LE, ME, and HE data respectively. Right panel: Data-to-model ratio plot of the six observations in Table 1 for 2-10 keV band. Different colors correspond to observations marked in the right panel of Figure 4. The vertical dashed lines mark the 6.4 keV iron Kα line rest energy.

Table 1 *Insight*-HXMT observations shown in Figure 6 right panel

ObsID	Date	Exposure (ks)	Count rate (cts/s)	Phase
004	20180324	28.7	1014	plateau
023	20180417	4.3	910	plateau
048	20180516	3.4	742	plateau
054	20180523	3.2	661	decay
060	20180531	4.4	540	decay
068	20180611	3.7	334	decay

Note – Only LE (1-10 keV) count rates are given.

We are also particularly interested in the transition between the "plateau" phase and the "decay" phase on the HID. The transition is marked by the sudden increase in hardness ratio. We choose six observations in total (three in the "plateau" phase and three in the "decay" phase), which span the entire hard state. Those observations are marked in Figure 1 and Figure 3 right panel, and are summarized in Table 3.2. We employed the simple power-law model to fit the 2-10 keV LE band. The data-to-model ratio is in Figure 6 right panel. As the source evolves from the "plateau" phase to the "decay" phase with decreasing luminosity, the iron line becomes broader while the red wing of it remains remarkably constant; the narrow core also gradually weakens.

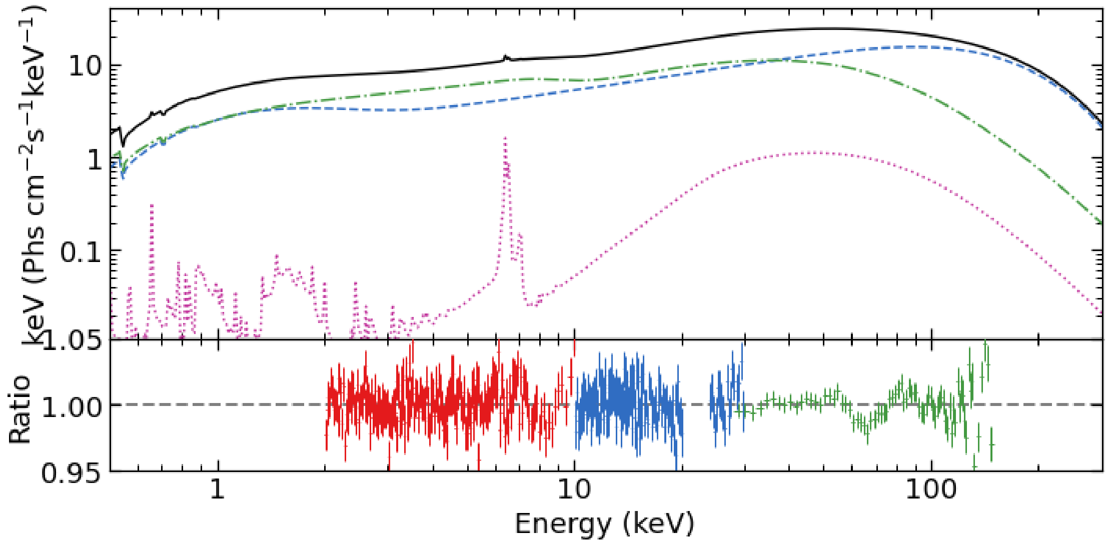

Figure 7. Best-fit model and data-to-model ratio of ObsID 007. Top panel: Solid black curve: the total model; blue dash-dotted curve: simplcut⊗diskbb; green dashed curve: relxilllpCp; purple dotted curve xillverCp. Bottom panel: Red points: LE; blue points: ME; green points: HE.

To account for the reflection features, we implement the reflection model relxilllpCp+xillverCp [32-33]. RelxilllpCp is a relativistic reflection model that assumes a lamppost geometry of the corona, i.e. a point-like source above the black hole at a height of h on its axis and calculates the illuminating pattern onto the disk directly from such geometry. XillverCp is the non-relativistic reflection model assuming a thermally Comptonized incident spectrum. In the ratio plot, a flux excess at 2-3 keV is also seen, which suggests a disk thermal component. We describe that with diskbb[34-35], a disk multi-temperature blackbody radiation model, and convolve it with model simplcutx[36], which takes the diskbb spectrum as the seed spectrum and returns the Comptonized component self-consistently. Therefore, the complete model is

$$\text{TBabs}\times(\text{simplcutx}\otimes\text{diskbb}+\text{relxilllpCp}+\text{xillverCp}).$$

To avoid the strong degeneracy between the black hole spin and the disk truncation radius [17], we fix the spin $a_* = 0.998$. Since it is expected that the distant disk region should have a lower ionization, while the thermally Comptonized spectrum should simultaneously serve as the incident spectrum for both the relativistic reflection and distant reflection, we tie the shared parameters between the two reflection components, except for the ionization and the flux normalization. Figure 7 shows the best-fit model and data-to-model ratio for ObsID 007 in the "plateau" phase.

4 Discussion and Summary

From the HID, the luminosity of the source gradually decreases in the "plateau" and "decay" phases, while the source re-brightens in the "transition" phase. The results from observations in those phases are marked by red, blue, and green circles hereafter.

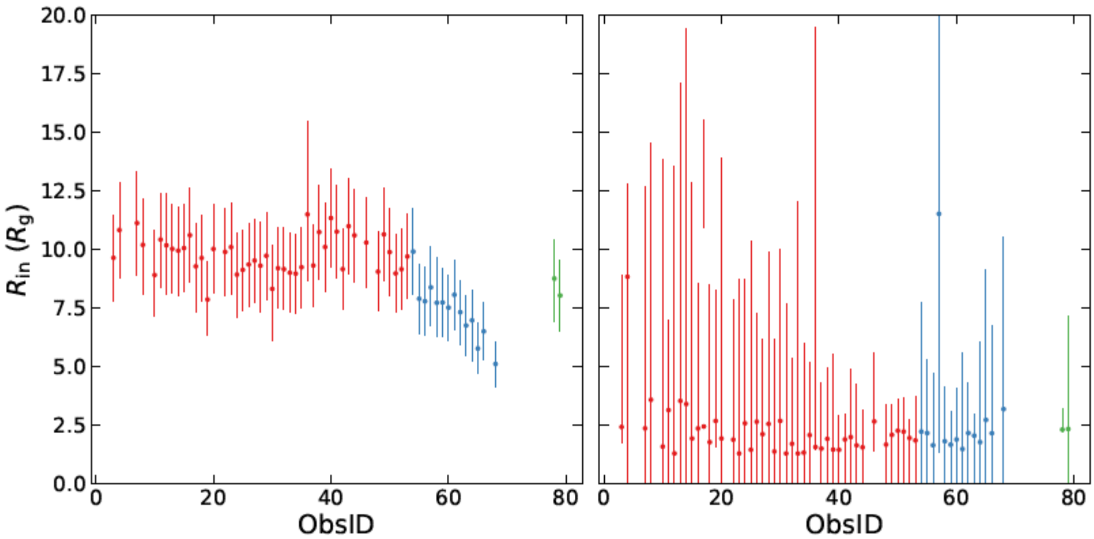

Figure 8. Left panel: Inner disk radius calculated from the normalization of diskbb model. Right panel: and from the reflection model. Observations in "plateau", "decay", and "transition" phases are marked by red, blue, and green points respectively.

4.1 Inner disk radius

We report the measured Rin with reflection in Figure 8 right panel. The constraints are relatively poor and in all observations Rin is close to ISCO. The measurement of Rin using reflection model is mostly based on the relativistic blurring of the iron $K\alpha$ line. As we assume a maximally spinning BH in our fits, there could be some systematic uncertainties in our measurement. In order to cross-check the results, we calculate Rin directly from the disk component, and we take this set of results in our analysis. The normalization of the diskbb model (N_{bb}) is based on the formula [35, 37]:

$$r_{in} = \sqrt{N_{bb}/\cos\theta} * D_{10} \tag{1}$$

where r_{in} is the apparent inner radius of the disk estimated from the spectrum, θ is the inclination angle, and D_{10} is the distance of the source in units of 10 kpc. The effective temperature of the disk T_{eff} is connected with the observed color temperature Tin by a factor of $1/f_{col}$, where f_{col} is the color correction factor[37]. The true inner radius of the disk Rin is related to the apparent inner radius by Eqn.(2) in[37]:

$$R_{in} = \xi' \cdot f_{col}^2 \cdot r_{in}, \tag{2}$$

where ξ' = 0.412 is the correction factor when the inner boundary condition is considered. We applied the "canonical" f_{col} value of 1.7 in [38]. We assume the inclination of (63 ± 3) deg, the source distance of (2.96 ± 0.33) kpc, and black hole mass of (9.2 ± 1.3) $M_{\odot}$ [39]. Rin calculated from the diskbb normalization is more constrained than that from reflection and their values are of the same order of magnitude, suggesting our models are self-consistent. If we assume a constant color correction factor over time, the results from the disk component show the inner radius is moderately truncated during all three phases if a maximally spinning BH ($a_* = 0.998$) is assumed. It stays almost constant ($10R_g$) in the "plateau" phase and slightly moves inward as the source enters the "decay" phase. The truncation is consistent with the truncated disk scenario of a typical outburst of a BH XRB in the hard state. In such a scenario, the disk is truncated away from the innermost stable circular orbit (ISCO) in the initial hard state, and the inner region is filled with a hot radiatively inefficient flow [40-41]. Then as the accretion rate increases, the disk component increases and the spectrum becomes softer; the disk moves inward until the source enters the HSS and the disk reaches ISCO[35]. However, the transition between the three phases in the hard state is peculiar as it does not fit into any canonical evolution pattern of BHBs. The inner radius Rin shows a shrinking trend in the "decay" phase. As we consider a constant f_{col}, the decreasing value of Rin would be associated with the decreasing trend of flux as indicated on the HID according to Eqn. (1) and Eqn. (2). This implies a relatively steady composition of spectral component and a less variable disk-corona structure compared with the "canonical" change in the system spanning the entire outburst.

We notice that our findings using disk modeling are consistent with [17], in which the inner radius is estimated by the reflection features, that the disk is close to ISCO in the hard state if we assume the standard $f_{col} = 1.7$. It is likely that fcol is well underestimated given the bright hard spectrum illuminates onto the disk in the hard state. This would imply a more truncated disk that is mildly affected by relativistic effect, consistent with the moderately blurred iron $K\alpha$ line shown in Figure 6 right panel.

We also note that a changing color correction factor f_{col} could also impact the estimate of Rin. An increasing f_{col} would lead to a decreasing Rin in the estimate. However,[42] and[43] both suggest a higher $f_{col}$when the disk fraction is less. The spectra of MAXI J1820+070 in the "decay" phase are slightly softer than the ones in the BHS where the corona illumination onto the disk is the strongest. This would suggest a much higher f_{col} in the BHS, and the decrease in R_{in} would be unlikely caused by an increasing f_{col}.

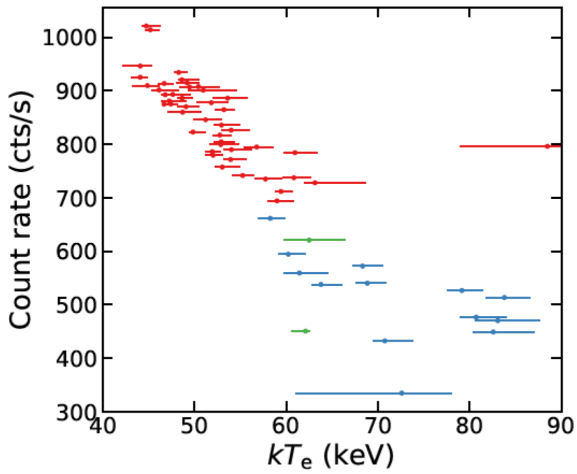

Figure 9. Count rate vs. corona temperature kT_e. A strong anti-correlation is observed. Observations in "plateau", "decay", and "transition" phases are marked by red, blue, and green points respectively.

4.2 QPO frequency and corona properties

For the correlation between QPO frequency and spectral parameters, we show the scatter plots between QPO frequency ν_{QPO} and the photon index Γ, the disk temperature at inner radius kT_{in}, and the disk inner radius Rin in Figure 11. We also show the count rate in LE 1-10 keV range versus the corona temperature in Figure 9, where a strong anti-correlation is observed. Such correlation has been observed in Active Galactic Nuclei (AGNs) and BHBs [44-45]. The trend can be explained by the corona scattering out more high energy photons as the luminosity increases, allowing sufficient photon collisions that lead to pair production, which plays a major role in determining the outgoing spectrum[46]. The temperature here is limited by pair production which overstrips annihilation and would radiates energy away [47].

ν_{QPO} and Γ are strongly correlated in each phase, but the exact dependence varies between different phases. The discrepancy in ν_{QPO}-Γ correlations between the two phases during an outburst is also observed by[48], who proposes that it results from different corona temperature. Such discrepancy between the temperature in the "plateau" and the "decay" phase has been confirmed in Figure 9, which further validates the claim. The disk temperature, however, does not show clear correlation with ν_{QPO} except for the initial BHS where ν_{QPO} rises (the bottom cluster of red points in the middle panel of Figure 11). Despite the ubiquity of LFQPO, its origin is still under debate. Many works have focused on the connection between the QPO frequency and the spectral parameters. The positive correlations between ν_{QPO} and Γ are frequently observed for BHBs[49-50]; correlations between ν_{QPO} and disk blackbody flux F_{disk} are also common [51]. However, as the hard continuum emitted from the corona is generated from the seed photons from the disk, there might be direct causality between the coronal emission and the disk emission, so we cannot simply identify the direct origin of the QPO solely based on the correlation study. If we could measure the correlation between the QPO and the spectral parameters when the causality between the corona and the disk is lifted, we might be able to break the degeneracy in correlations. In the disk-corona model, the spectrum of the Comptonized photons is determined by the corona temperature kT_e and the optical depth of Thompson scattering τ. When the energy is much lower than kT_e, the hard powerlaw spectrum, $F(E) \propto E^{1-\Gamma}$, is created through multiple scatterings of photons in the corona, where the emitted hard spectrum might be insensitive to the seed photons if the optical depth is large enough[52]. When $kT_e \ll m_e c^2$ and $\tau^2 \gg 1$, the powerlaw photon index is given by[53]

$$\Gamma = \sqrt{\frac{9}{4} + \frac{\pi^2 m_e c^2}{3kT_e\left(\tau+\frac{2}{3}\right)^2}} \tag{3}$$

Indeed we do not see the dependence of Γ on the disk temperature kT_{in}. This suggests that if we consider the case where $\tau^2 \gg 1$, then we could eliminate the intrinsic correlation between Γ and kT_e occurs in the Comptonization, so that we could compare how the QPO frequency varies with these two parameters. To illustrate the evolution of τ during the outburst, we plot the contours of τ on the $\Gamma - kT_{in}$ plane according to Eqn. (13) in [54], and put our data points above it in Figure 10 left panel. Figure 10 right panel shows Γ versus kT_{in}. For observations in the "plateau" phase, when $\Gamma < 1.55$ and $\tau > 2.5$, Γ and kT_{in} do not show any correlation, while in Figure 11 the νQPO-Γ correlation is well observed while ν_{QPO}- kT_{in} is not. This evidence excludes the direct causality connection between Γ and kT_{in} and thus supports the corona to be the source of the LFQPO.

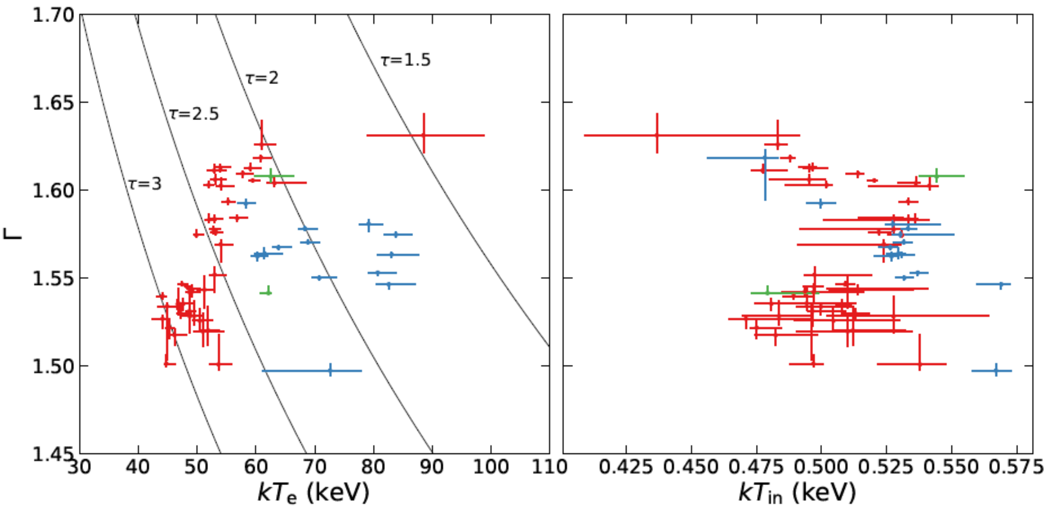

Figure 10: Left panel: Powerlaw photon index Γ versus corona temperature kT_e. The black solid curves are the contours of the optical depth τ based on Eqn. (13) in [54]. Right panel: Powerlaw photon index Γ versus disk temperature kT_{in}. Observations in "plateau", "decay", and "transition" phases are marked by red, blue, and green

points respectively.

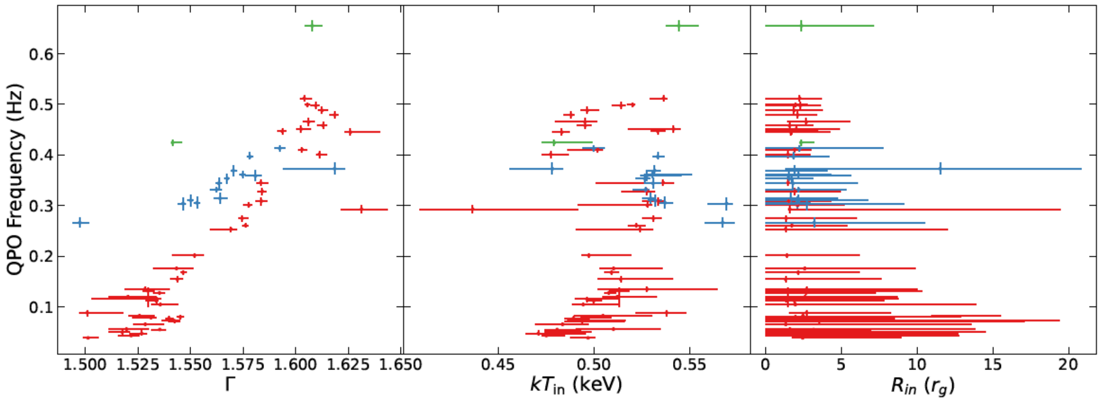

Figure 11: QPO frequency ν_{QPO} against spectral parameters. Left panel: pho- ton index Γ; middle panel: disk temperature at inner radius kT_{in}; right panel: disk inner radius given by reflection.

4.3 Conclusion

Utilizing the broad-band energy coverage, the good timing capability, and the large number of available data sets of *Insight*-HXMT, we have conducted a detailed spectral-timing analysis of the 2018 outburst of a bright black hole X-ray binary MAXI J1820+070. By combining self-consistent spectral modeling and well-developed timing techniques, we are able to extract the behavior of the disk-corona system and identify the origin of LFQPO in the corona.

MAXI J1820+070 is an interesting source that has an extremely bright hard state in which we are particularly interested. During the hard state, the source exhibits peculiar transitions between small "phases" that resembles a typical "q" pattern on the HID. We identify the observations in the hard state into three phases. The red-wing of the iron Kα line, and the measured inner radius of the disk using self-consistent disk emission modeling are both remarkably stable, suggesting a constant disk properties during the hard state. The spectral change during the hard state is mainly due to a change in the corona emission. LFQPOs are mainly discovered in the hard state with frequency ν_{QPO} below 0.5 Hz. ν_{QPO} is strongly correlated with the hard powerlaw continuum photon

index during the bright "plateau" phase, and the existence of QPOs up to 200 keV is consistent with the claim in[27]. After eliminating the condition where the corona emission directly correlates with the disk emission, we find a strong ν_{QPO}-Γ correlation while there is not clear ν_{QPO}-kT_{in} correlation. Together with the presence of QPO at high energy, we identify that LFQPO as a phenomenon that originates from the corona. We stress that the spectral-timing behavior of MAXI J1820+070 could be simultaneously explained by the corona.

Acknowledgment: This work was supported by Hui-Chun Chin and Tsung-Dao Lee Chinese Undergraduate Research Endowment (CURE) and Summer Undergraduate Research Fellowship

(SURF) at Caltech, and was conducted with members of the *NuSTAR* working group at Caltech. We thank the inspiring discussions with Matteo Bachetti, and the members in the spectral-timing telecon, the NuSTAR group, and the Institute of High Energy Physics at Beijing.

References

[1] BELLONI T M, MOTTA S E, MUNˇOZ-DARIAS T. 2011. arXiv: 1109.3 388 [astro-ph.HE].

[2] MOTTA S E. Quasi periodic oscillations in black hole binaries[J/OL]. Astronomische Nachrichten, 2016, 337(4-5): 398-403. http://dx.doi.org/1 0.1002/asna.201612320. DOI: 10.1002/asna.201612320.

[3] STELLA L, VIETRI M. Lense-Thirring Precession and Quasi-periodic Oscillations in Low-Mass X-Ray Binaries[J]., 1998, 492(1): L59-L62. arXiv: astro-ph/9709085 [astro-ph]. DOI: 10.1086/311075.

[4] INGRAM A, DONE C, FRAGILE P C. Low-frequency quasi-periodic oscillations spectra and Lense-Thirring precession[J]., 2009, 397(1): L101- L105. arXiv: 0901.1238 [astro-ph.SR]. DOI: 10.1111/j.1745-3933.2009.00693.x.

[5] TAGGER M, PELLAT R. An accretion-ejection instability in magnetized disks[J]., 1999, 349: 1003-1016. arXiv: astro-ph/9907267 [astro-ph].

[6] CABANAC C, HENRI G, PETRUCCI P O, et al. Variability of X-ray binaries from an oscillating hot corona[J/OL]., 2010, 404(2): 738-748. htt p://dx.doi.org/10.1111/j.1365-2966.2010.16340.x. DOI: 10.1111/j.1365-2 966.2010.16340.x.

[7] INGRAM A, MOTTA S. A review of quasi-periodic oscillations from black hole X-ray binaries: observation and theory[Z]. 2020. arXiv: 2001.08758 [astro-ph.HE].

[8] SOBOLEWSKA M A, Z˙ YCKI P T. Spectral and Fourier analyses of X-ray quasi-periodic oscillations in accreting black holes[J/OL]., 2006, 370(1): 405-414. eprint: https://academic.oup.com/mnras/article-pdf/370/1/405/3417181/mnras0370-0405.pdf. https://doi.org/10.1111/j.1365-2966.200 6.10489.x. DOI: 10.1111/j.1365-2966.2006.10489.x.

[9] SHAPOSHNIKOV N, TITARCHUK L. Determination of Black Hole Mass in Cygnus X-1 by Scaling of Spectral Index–QPO Frequency Correla- tion[J/OL]., 2007, 663(1): 445-449. http://dx.doi.org/10.1086/518110. DOI: 10.1086/518110.

[10] TITARCHUK L, FIORITO R. Spectral Index and Quasi-Periodic Oscilla- tion Frequency Correlation in Black Hole Sources: Observational Evidence of Two Phases and Phase Transition in Black Holes[J/OL]., 2004, 612(2): 988-999. http://dx.doi.org/10.1086/422573. DOI: 10.1086/422573.

[11] SHAPPEE B J, PRIETO J L, GRUPE D, et al. The Man behind the Curtain: X-Rays Drive the UV through NIR Variability in the 2013 Active Galactic Nucleus Outburst in NGC 2617[J]., 2014, 788(1), 48: 48. arXiv: 1310.2241 [astro-ph.HE]. DOI: 10.1088/0004-637X/788/1/48.

[12] MATSUOKA M, KAWASAKI K, UENO S, et al. The MAXI Mission on the ISS: Science and Instruments for Monitoring All-Sky X-Ray Images[J]., 2009, 61: 999. arXiv: 0906.0631 [astro-ph.IM]. DOI: 10.1093/pasj/61.5.999.

[13] SHIDATSU M, NAKAHIRA S, MURATA K L, et al. X-Ray and Optical Monitoring of State Transitions in MAXI J1820+070[J]., 2019, 874(2), 183: 183. arXiv: 1903.01686 [astro-ph.HE]. DOI: 10.3847/1538-4357/ab 09ff.

[14] GENDREAU K C, ARZOUMANIAN Z, ADKINS P W, et al. The Neu- tron star Interior Composition Explorer (NICER): design and develop- ment[C]//DEN HERDER J W A, TAKAHASHI T, BAUTZ M. Society of Photo-Optical Instrumentation Engineers (SPIE) Conference Series: Space Telescopes and Instrumentation 2016: Ultraviolet to Gamma Ray: vol. 9905. [S.l. : s.n.], 2016: 99051H. DOI: 10.1117/12.2231304.

[15] KARA E, STEINER J F, FABIAN A C, et al. The corona contracts in a black-hole transient[J]., 2019, 565(7738): 198-201. arXiv: 1901.03877 [astro-ph.HE]. DOI: 10.1038/s41586-018-0803-x.

[16] WANG J, MASTROSERIO G, KARA E, et al. Disk, Corona, Jet Connec- tion in the Intermediate State of MAXI J1820+070 Revealed by NICER
Spectral-timing Analysis[J]., 2021, 910(1), L3: L3. arXiv: 2103.05616 [astro-ph.HE]. DOI: 10.3847/2041-8213/abec79.

[17] BUISSON D J K, FABIAN A C, BARRET D, et al. MAXI J1820+070 with NuSTAR I. An increase in variability frequency but a stable reflection spectrum: coronal properties and implications for the inner disc in black hole binaries[J]., 2019, 490(1): 1350-1362. arXiv: 1909.04688 [astro-ph.HE]. DOI: 10.1093/mnras/stz2681.

[18] HARRISON F A, CRAIG W W, CHRISTENSEN F E, et al. The Nuclear Spectroscopic Telescope Array (NuSTAR) High-energy X-Ray Mission[J]., 2013, 770(2), 103: 103. arXiv: 1301.7307 [astro-ph.IM]. DOI: 10.1088/0 004-637X/770/2/103.

[19] ZHANG S N, LI T, LU F, et al. Overview to the Hard X-ray Modula- tion Telescope (Insight-HXMT) Satellite[J]. Science China Physics, Me- chanics, and Astronomy, 2020, 63(4), 249502: 249502. arXiv: 1910.09613 [astro-ph.IM]. DOI: 10.1007/s11433-019-1432-6.

[20] CHEN Y, CUI W, LI W, et al. The Low Energy X-ray telescope (LE) onboard the Insight-HXMT astronomy satellite[J]. Science China Physics, Mechanics, and Astronomy, 2020, 63(4), 249505: 249505. arXiv: 1910.083 19 [astro-ph.IM]. DOI: 10.1007/s11433-019-1469-5.

[21] CAO X, JIANG W, MENG B, et al. The Medium Energy X-ray telescope (ME) onboard the

Insight-HXMT astronomy satellite[J]. Science China Physics, Mechanics, and Astronomy, 2020, 63(4), 249504: 249504. DOI: 10.1007/s11433-019-1506-1.

[22] LIU C, ZHANG Y, LI X, et al. The High Energy X-ray telescope (HE) onboard the Insight-HXMT astronomy satellite[J]. Science China Physics, Mechanics, and Astronomy, 2020, 63(4), 249503: 249503. arXiv: 1910.049 55 [astro-ph.IM]. DOI: 10.1007/s11433-019-1486-x.

[23] LIAO J Y, ZHANG S, LU X F, et al. Background model for the high- energy telescope of Insight-HXMT[J]. Journal of High Energy Astrophysics, 2020, 27: 14-23. arXiv: 2005.01661 [astro-ph.IM]. DOI: 10.1016/j.jheap.2020.04.002.

[24] GUO C C, LIAO J Y, ZHANG S, et al. The background model of the medium energy X-ray telescope of Insight-HXMT[J]. Journal of High En- ergy Astrophysics, 2020, 27: 44-50. arXiv: 2003 . 06260 [astro-ph.IM]. DOI: 10.1016/j.jheap.2020.02.008.

[25] LIAO J Y, ZHANG S, CHEN Y, et al. Background model for the Low- Energy Telescope of Insight-HXMT[J]. Journal of High Energy Astro- physics, 2020, 27: 24-32. arXiv: 2004.01432 [astro-ph.IM]. DOI: 10.101 6/j.jheap.2020.02.010.

[26] HUPPENKOTHEN D, BACHETTI M, STEVENS A L, et al. Stingray: A Modern Python Library for Spectral Timing[J]., 2019, 881(1), 39: 39. arXiv: 1901.07681 [astro-ph.IM]. DOI: 10.3847/1538-4357/ab258d.

[27] MA X, TAO L, ZHANG S N, et al. Discovery of oscillations above 200 keV in a black hole X-ray binary with Insight-HXMT[J]. Nature Astronomy, 2021, 5: 94-102. arXiv: 2009.10607 [astro-ph.HE]. DOI: 10.1038/s41550-020-1192-2.

[28] ARNAUD K A. XSPEC: The First Ten Years[C]//JACOBY G H, BARNES J. Astronomical Society of the Pacific Conference Series: Astronomical Data Analysis Software and Systems V: vol. 101. [S.l. : s.n.], 1996: 17.

[29] VERNER D A, FERLAND G J, KORISTA K T, et al. Atomic Data for Astrophysics. II. New Analytic FITS for Photoionization Cross Sections of Atoms and Ions[J]., 1996, 465: 487. arXiv: astro-ph/9601009 [astro-ph]. DOI: 10.1086/177435.

[30] WILMS J, ALLEN A, MCCRAY R. On the Absorption of X-Rays in the Interstellar Medium[J]., 2000, 542(2): 914-924. arXiv: astro- ph/0008425 [astro-ph]. DOI: 10.1086/317016.

[31] UTTLEY P, GENDREAU K, MARKWARDT C, et al. NICER observa- tions of MAXI J1820+070 suggest a rapidly-brightening black hole X-ray binary in the hard state[J]. The Astronomer's Telegram, 2018, 11423: 1.

[32] DAUSER T, GARCIA J, PARKER M L, et al. The role of the reflection fraction in constraining black hole spin.[J]., 2014, 444: L100-L104. arXiv: 1408.2347 [astro-ph.HE]. DOI: 10.1093/mnrasl/slu125.

[33] GARCIA J, DAUSER T, LOHFINK A, et al. Improved Reflection Models of Black Hole Accretion Disks: Treating the Angular Distribution of X- Rays[J]., 2014, 782(2), 76: 76. arXiv: 1312.3231 [astro-ph.HE]. DOI: 10.1088/0004-637X/782/2/76.

[34] MITSUDA K, INOUE H, KOYAMA K, et al. Energy spectra of low-mass binary X-ray sources observed from Tenma.[J]., 1984, 36: 741-759.

[35] MAKISHIMA K, MAEJIMA Y, MITSUDA K, et al. Simultaneous X-Ray and Optical Observations of GX 339-4 in an X-Ray High State[J]., 1986, 308: 635. DOI: 10.1086/164534.

[36] STEINER J F, GARCIA J A, EIKMANN W, et al. Self-consistent Black Hole Accretion Spectral Models and the Forgotten Role of Coronal Comp- tonization of Reflection Emission[J]., 2017, 836(1), 119: 119. arXiv: 1701.03777 [astro-ph.HE]. DOI: 10.3847/1538-4357/836/1/119.

[37] KUBOTA A, TANAKA Y, MAKISHIMA K, et al. Evidence for a Black Hole in the X-Ray Transient GRS 1009-45[J]., 1998, 50: 667-673. DOI: 10.1093/pasj/50.6.667.

[38] SHIMURA T, TAKAHARA F. On the Spectral Hardening Factor of the X-Ray Emission from Accretion Disks in Black Hole Candidates[J]., 1995, 445: 780. DOI: 10.1086/175740.

[39] ATRI P, MILLER-JONES J C A, BAHRAMIAN A, et al. A radio parallax to the black hole X-ray binary MAXI J1820+070[J]., 2020, 493(1): L81- L86. arXiv: 1912.04525 [astro-ph.HE]. DOI: 10.1093/mnrasl/slaa010.

[40] ESIN A A, MCCLINTOCK J E, NARAYAN R. Advection-Dominated Ac- cretion and the Spectral States of Black Hole X-Ray Binaries: Application to Nova Muscae 1991[J]., 1997, 489(2): 865-889. arXiv: astro-ph/9705237 [astro-ph]. DOI: 10.1086/304829.

[41] NARAYAN R, YI I, MAHADEVAN R. Explaining the spectrum of Sagit- tarius A∗ with a model of an accreting black hole[J]., 1995, 374(6523): 623-625. DOI: 10.1038/374623a0.

[42] MERLONI A, FABIAN A C, ROSS R R. On the interpretation of the multicolour disc model for black hole candidates[J]., 2000, 313(1): 193- 197. arXiv: astro-ph/9911457 [astro-ph]. DOI: 10.1046/j.1365-8711.20 00.03226.x.

[43] DUNN R J H, FENDER R P, KO¨ RDING E G, et al. A global study of the behaviour of black hole X-ray binary discs[J]., 2011, 411(1): 337-348. arXiv: 1009.2599 [astro-ph.HE]. DOI: 10.1111/j.1365-2966.2010.17687.x.

[44] JOINET A, KALEMCI E, SENZIANI F. Hard X-Ray Emission of the Microquasar GRO J1655-40 during the Rise of Its 2005 Outburst[J]., 2008, 679(1): 655-663. arXiv: 0803.3934 [astro-ph]. DOI: 10.1086/533512.

[45] LUBIN´SKI P, ZDZIARSKI A A, WALTER R, et al. Extreme flux states of NGC 4151 observed with INTEGRAL[J]., 2010, 408(3): 1851-1865. arXiv: 1005.0842 [astro-ph.CO]. DOI: 10.1111/j.1365-2966.2010.17251.x.

[46] SVENSSON R, ZDZIARSKI A A. Black Hole Accretion Disks with Coro- nae[J]., 1994, 436: 599. DOI: 10.1086/174934.

[47] FABIAN A C, LOHFINK A, KARA E, et al. Properties of AGN coro- nae in the NuSTAR era[J]., 2015, 451(4): 4375-4383. arXiv: 1505 . 07603 [astro-ph.HE]. DOI: 10.1093/mnras/stv1218.

[48] SHAPOSHNIKOV N, JAHODA K, MARKWARDT C, et al. ADVANCES IN THERXTEPROPORTIONAL COUNTER ARRAY CALIBRATION: NEARING THE STATISTICAL LIMIT[J/OL]., 2012, 757(2): 159. https://doi.org/10.1088/0004-637x/757/2/159. DOI: 10.1088/0004-637x/757/2/159.

[49] FU¨ RST F, GRINBERG V, TOMSICK J A, et al. Spectro-Timing Study of GX 339-4 in a Hard Intermediate State[J]., 2016, 828(1), 34: 34. arXiv: 1604.08644 [astro-ph.HE]. DOI: 10.3847/0004-637X/828/1/34.

[50] VIGNARCA F, MIGLIARI S, BELLONI T, et al. Tracing the power-law component in the energy spectrum of black hole candidates as a function of the QPO frequency[J]., 2003, 397: 729-738. arXiv: astro- ph/ 0210517 [astro-ph]. DOI: 10.1051/0004-6361:20021542.

[51] MUNO M P, MORGAN E H, REMILLARD R A. Quasi-periodic Oscil- lations and Spectral States in GRS 1915+105[J]., 1999, 527(1): 321-340. DOI: 10.1086/308063.

[52] BAMBI C, BRENNEMAN L W, DAUSER T, et al. Towards Precision Measurements of Accreting Black Holes Using X-Ray Reflection Spectroscopy[J]., 2021, 217(5), 65: 65. arXiv: 2011.04792 [astro-ph.HE]. DOI: 10.1007/s11214-021-00841-8.

[53] SUNYAEV R A, TITARCHUK L G. Comptonization of X-Rays in Plasma Clouds - Typical Radiation Spectra[J]., 1980, 86: 121.

[54] BELOBORODOV A M. Accretion Disk Models[C]//POUTANEN J, SVENSSON R. Astronomical Society of the Pacific Conference Series: High Energy Processes in Accreting Black Holes: vol. 161. [S.l. : s.n.], 1999: 295. arXiv: astro-ph/9901108 [astro-ph].